

Journal of Biomedical Optics

BiomedicalOptics.SPIEDigitalLibrary.org

On the interpretation of second harmonic generation intensity profiles of striated muscle

Rik Paesen
Sophie Smolders
Inez Wens
Kristof Notelaers
José Manolo de Hoyos Vega
Virginie Bito
Bert O. Eijnde
Dominique Hansen
Marcel Ameloot

On the interpretation of second harmonic generation intensity profiles of striated muscle

Rik Paesen,^a Sophie Smolders,^a Inez Wens,^{a,b} Kristof Notelaers,^a José Manolo de Hoyos Vega,^a Virginie Bito,^a Bert O. Eijnde,^{a,b} Dominique Hansen,^{a,b} and Marcel Ameloot^{a,*}

^aHasselt University, Biomedical Research Institute, Agoralaan Building C, Diepenbeek 3590, Belgium

^bHasselt University, REVAL—Rehabilitation Research Center, Agoralaan Building A, Diepenbeek 3590, Belgium

Abstract. Recently, a supramolecular model was developed for predicting striated skeletal muscle intensity profiles obtained by label-free second harmonic generation (SHG) microscopy. This model allows for a quantitative determination of the length of the thick filament antiparallel range or M-band (M), and results in $M = 0.12 \mu\text{m}$ for single-band intensity profiles when fixing the A-band length (A) to $A = 1.6 \mu\text{m}$, a value originating from electron microscopy (EM) observations. Using simulations and experimental data sets, we showed that the objective numerical aperture (NA) and the refractive index (RI) mismatch ($\Delta n = n_{2\omega} - n_{\omega}$) between the illumination wave (ω) and the second harmonic wave (2ω) severely affect the simulated sarcomere intensity profiles. Therefore, our recovered filament lengths did not match with those observed by EM. For an RI mismatch of $\Delta n = 0.02$ and a moderate illumination NA of 0.8, analysis of single-band SHG intensity profiles with freely adjustable A- and M-band sizes yielded $A = 1.40 \pm 0.04 \mu\text{m}$ and $M = 0.07 \pm 0.05 \mu\text{m}$ for skeletal muscle. These lower than expected values were rationalized in terms of the myosin density distribution along the myosin thick filament axis. Our data provided new and practical insights for the application of the supramolecular model to study SHG intensity profiles in striated muscle. © 2015 Society of Photo-Optical Instrumentation Engineers (SPIE) [DOI: 10.1117/1.JBO.20.8.086010]

Keywords: striated muscle; second harmonic generation; refractive index; supramolecular model.

Paper 150262R received Apr. 20, 2015; accepted for publication Jul. 21, 2015; published online Aug. 17, 2015.

1 Introduction

Second harmonic generation (SHG) microscopy has been demonstrated to be an excellent tool for label-free imaging of several biological structures. The well-defined properties of the SHG signal makes it convenient to study well-ordered structures, such as collagen type I rich structures,^{1–4} microtubules inside mitotic spindles or neurons^{5–7} and striated muscle containing myosin thick filaments.^{8–11} SHG microscopy relies on the presence of noncentrosymmetric features, achieved through a high degree of order of polar biomolecules. This implies that even the smallest changes in this structural regularity have detrimental effects on the resulting SHG signals, making SHG microscopy one of the tools for early detection of the reorganization of SHG active molecules.

Disorder of otherwise perfectly aligned myosin thick filaments is known to occur within muscle tissue, either as a primary consequence of muscle targeting disease, such as Nemalin myopathy¹² or Pompe's disease,¹³ or as secondary effects of muscle disuse.¹⁴ Various studies have recently emerged, suggesting SHG microscopy to be a valuable label-free tool to study muscular disorder.^{13,15,16} However, to fully understand the effect of muscle degradation on the SHG signal, detailed knowledge of sarcomere structures and their relation to the second harmonic signal generation is necessary.

Striped SHG patterns are typical for skeletal and cardiac muscle.^{9–11,17} Two SHG-based approaches have been used to

quantify these striations.^{9,16,18} Both methods are based on analyzing a one-dimensional intensity profile, mostly extracted from two-dimensional SHG images. The first approach relies on a phenomenological profile definition such as a double Gaussian peak.^{16,18} This is useful for analyzing double peaked intensity profiles observed in cardiac muscle tissue, but apart from the sarcomere length, the resulting parameter values have no direct relation to the biological structural properties of sarcomeres. The second approach is developed by Rouède et al.⁹ and relies on a more rigorous model based on the molecular organization of sarcomeres. Starting from the Maxwell equations, they derive electric field expressions for far-field SHG radiation to predict intensity profiles. In this so called supramolecular model, the SHG signal is assumed to originate from the thick filament (A-band), consisting of two oppositely directed noncentrosymmetric hemifilaments. This reversed directionality leads to a π phase difference between the SHG signals coming from both hemifilaments and makes the thick filament centrosymmetric where the hemifilaments connect and overlap (M-band). By including these features, the model comprises the A-band length (A), M-band length (M), and sarcomere length (L) as biological structural parameters [Fig. 1(a)]. Besides these structural parameters, microscope-related parameters, such as the optical point spread function (PSF) and the numerical aperture (NA) of the signal collection optics, are implemented in the model.

To use the supramolecular model, Rouède et al.⁹ sets the A-band length to $A = 1.6 \mu\text{m}$, a generally accepted value

*Address all correspondence to: Marcel Ameloot, E-mail: marcel.ameloot@uhasselt.be

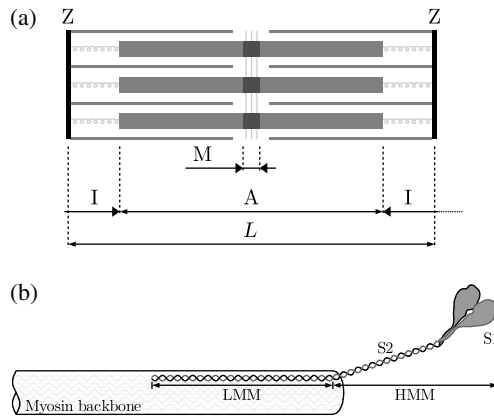


Fig. 1 (a) Illustration of sarcomere structure. L is the sarcomere length from Z-line to Z-line, A is the thick filament A-band, M is the antiparallel M-region, I indicates the I-band. (b) Detailed depiction of the right end of a thick filament. It shows how the light meromyosin (LMM) chain contributes to the myosin backbone, whereas subfragments 1 (S1) and 2 (S2) of the heavy meromyosin (HMM) are not part of this backbone due to a loose S2/LMM hinge connection.

observed by electron microscopy (EM).^{19,20} Fitting the experimental profiles yields the sarcomere length and the M-band size as biologically relevant parameters. For healthy skeletal muscle tissue, consisting of single-peaked SHG intensity profiles, an M-band length of $M = 0.12 \mu\text{m}$ results,⁹ which is smaller than the EM-related value of $M = 0.15 \mu\text{m}$, as previously described.^{19,20} This shorter length is assumed to be a consequence of unaccounted for spherical aberrations.⁹ However, when applying the supramolecular model as suggested by Rouède et al.,⁹ we observed severe experimental versus theoretical profile discrepancies.

The aim of our study was, therefore, to determine the apparent A- and M-band lengths obtained from SHG data using the supramolecular model when A is set as a freely adjustable parameter, instead of fixing it to $1.6 \mu\text{m}$. This yielded more accurate fits, but both the apparent A- and M-band lengths were then lower than their corresponding EM values, with M-band lengths approaching zero. To explain the obtained values, we studied the effect of two optical parameters and a biological feature on the SHG intensity profiles of sarcomeres.

The first optical parameter is the refractive index (RI) mismatch between the illumination wavelength (n_ω) and the SHG wavelength ($n_{2\omega}$). Rouède et al.⁹ assumes that the RI of muscle tissue approaches that of water and that the tissue behaves in a dispersionless manner: $n_\omega = n_{2\omega} = 1.33$. However, even a small RI mismatch already leads to a signal phase mismatch in the axial direction,²¹ affecting the coherent properties of the SHG signal, and thereby altering the far-field emission profile on which the supramolecular model relies. RI data for muscle tissue originating from various species have been reported, mentioning values ranging from 1.37 to 1.41 in the visible wavelength range.^{22–24} Yet only a limited number of studies exist where a full dispersion analysis from the visible to near infrared light range is performed.²³ Besides the regular wavelength dependence of the RI, other RI affecting optical effects might be involved. The use of not only ultrashort pulsed lasers²⁵ but also dichroism²⁴ and differences in the RI of the sarcomere A and I region²⁶ play a role in the complete dispersion properties of skeletal muscle tissue. In this study, we investigated the

dispersion effect by analyzing an experimental data set with a range of RI mismatches.

The second optical parameter that affects the returned length information is the NA of the illumination objective. To obtain sufficient resolution for an accurate length estimate, immersion objectives with higher NAs are desired. However, tighter focusing with high NA objectives induces additional transverse and axial polarization fields,^{27,28} which are not included in the supramolecular model.⁹ We, therefore, looked at the influence of the illumination NA on the returned lengths.

The studied biological feature is related to the ordering of the myosin rods inside the thick filament. For this, the effect of the density distribution of myosin rods along the thick filament axis was studied. We performed simulations by implementing the myosin packing according to models by Knight et al.²⁹ and Skubiszak and Kowalczyk,³⁰ considering either the LMM or the LMM and S2 as SHG active regions (Fig. 1).^{8,11,31}

2 Materials and Methods

2.1 Tissue Preparation

2.1.1 Skeletal muscle

Female Lewis rats of age 6 to 7 weeks and body weight 100 to 120 g (Harlan CPB, Zeist, The Netherlands) were housed in the animal facilities at Hasselt University. The animals used in this work were the health control animals of a study for which the protocol was approved by the animal Ethics Committee of Hasselt University and which was in accordance with the national and European legislation. The National Research Council's guide for the care and use of laboratory animals was followed.

After anesthetizing with pentobarbital sodium (5 mg/100 g body weight), *Flexor digitorum longus* muscles were dissected from both hind limbs, incubated overnight in 4% paraformaldehyde (PFA) at 4°C, followed by cryoprotection in 30% sucrose in phosphate buffered saline (PBS) at 4°C until the tissue had sunk. Muscles were frozen in optimal cutting temperature compound (Tissue-Tek, Sakura Finetek Europe, The Netherlands) using liquid nitrogen cooled isopentane and stored at -80°C . About $14\text{-}\mu\text{m}$ thick sections were cut on a cryostat (CL 1990 UV, Leica, Wetzlar, Germany) along the length of the myofibers, mounted onto Superfrost Plus glasses (Menzel-Gläser, Thermo Fisher Scientific, Waltham, Massachusetts), and stored at -20°C . Before imaging, sections were washed three times for 5 min in PBS, dipped into milli-Q water, and a cover slip was placed using Immu-Mount™ (Thermo Fisher Scientific). Cover-slipped sections were stored at 4°C until imaging.

2.2 Microscopy

SHG imaging was performed using a Zeiss LSM510 META (Carl Zeiss, Jena, Germany) mounted on an Axiovert 200M and a $40\times/1.3$ oil immersion objective (Plan-Neofluar $40\times/1.3$ Oil DIC, Carl Zeiss). A back aperture pinhole was used to reduce the effective NA to ~ 0.8 in order to be able to test the effect of a higher NA on the recovered model parameters.²⁷ The excitation was provided by a femtosecond pulsed laser (MaiTai DeepSee, Spectra-Physics, California) tuned at a central wavelength of $\lambda_\omega = 810 \text{ nm}$. The SHG signal was collected in the forward mode by a condenser with a NA_c of 0.8. After passing through a 400- to 410-nm bandpass filter, the forward directed signal was detected by an analogue photomultiplier tube, delivered by Zeiss.

2.3 Point Spread Function

The PSF was measured by two-photon excited fluorescence microscopy of green fluorescent microspheres (PS-Speck™ Microscope Point Source Kit, Molecular Probes, Eugene, Oregon) mounted on a microscope cover glass. The three-dimensional (3-D) PSF information of at least 20 beads was compared to a 3-D Gaussian intensity profile for two-photon processes (I_{2P}):

$$I_{2P}(x, y, z) \propto |E_{\omega}(x, y, z)|^4 \propto e^{-\frac{4x^2+4y^2}{w_{xy}^2} - \frac{4z^2}{w_z^2}}, \quad (1)$$

yielding $w_{xy} = 0.576 \mu\text{m}$ and $w_z = 3.802 \mu\text{m}$ for $\text{NA} = 0.8$, and $w_{xy} = 0.467 \mu\text{m}$ and $w_z = 1.946 \mu\text{m}$ for $\text{NA} = 1.3$.

2.4 Sarcomere Profile Analysis

The profile analysis was done by in-house developed MATLAB (Version R2013a, The MathWorks, Natick, Massachusetts) routines. Sarcomere dimensions were obtained by analysis of manually selected intensity profiles. Each selected profile was required to extend to at least three similarly appearing sarcomeres to obtain a good estimate of all length parameters. Four additional parallel profiles separated one pixel, and two pixels at both sides of the selected profile were included and averaged for noise reduction. Cubic interpolation was used by MATLAB's built-in function "improfile" to obtain SHG intensities for the coordinates belonging to the selected profile. The weighted and reduced goodness-of-fit (χ^2) for each profile was calculated by taking the experimentally determined noise properties of the imaging set up into account. The intensity-dependent noise was quantified by calculating the mean and standard deviation from a series of uniform images.

2.5 Simulations

Myosin density simulations were performed for an illumination NA of 0.8, using a sarcomere length of $L = 2.2 \mu\text{m}$ and a RI mismatch of $\Delta n = 0.02$ with $n_{\omega} = 1.39$, based on the results shown in Sec. 3.1. For repeated simulations, random noise obeying the measured noise properties was superimposed onto a noise-free profile.

2.6 Supramolecular Model

The SHG far field radiation pattern was calculated by⁹

$$I(\theta, \phi) \sim I^X I^Y I^Z (1 - \sin^2 \theta \cos^2 \phi), \quad (2)$$

where θ and ϕ represents the polar and azimuthal angles, respectively, with respect to the center of the Gaussian illumination beam (Fig. 2). The dispersion-induced phase mismatch between the illumination wave ($k_{\omega} = 2\pi n_{\omega} \lambda_{\omega}^{-1}$) and the SHG signal ($k_{2\omega} = 4\pi n_{2\omega} \lambda_{\omega}^{-1}$), has an effect on the X, Y, and Z components, which are given by^{9,32}

$$I^X = \frac{\pi}{2} w_{xy}^2 \left| \sum_{n=-\infty}^{+\infty} a_{\Delta, n} e^{-\frac{1}{8} k_{2\omega}^2 w_{xy}^2 (\sin \theta \cos \phi - \frac{2n\pi}{L k_{2\omega}})^2} \right|^2, \quad (3)$$

$$I^Y = \frac{\pi}{2} w_{xy}^2 e^{-\frac{1}{4} k_{2\omega}^2 w_{xy}^2 (\sin \theta \sin \phi)^2}, \quad (4)$$

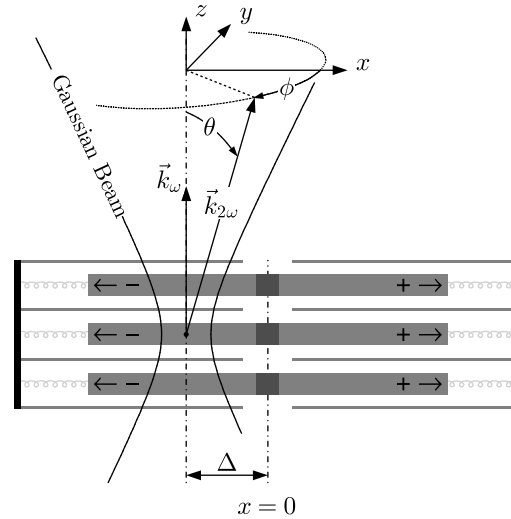


Fig. 2 Parameters in the supramolecular model and system definition. Δ is the scan parameter representing the position of the Gaussian beam with respect to the center of the sarcomere. The + and - signs represent the π phase shift due to the direction inversion at the center of the thick filament, as indicated by the arrows. See Fig. 1 for the definition of the structural parameters A , M , and L .

$$I^Z = \frac{\pi}{2} w_z^2 e^{-\frac{1}{4} w_z^2 (k_{2\omega} \cos \theta - 2k_{\omega} + 4k_{\omega}^{-1} w_{xy}^{-2})^2} \quad (5)$$

with

$$a_{\Delta, n} = \frac{-2i}{\pi n} \sin \left[\pi n \frac{A+M}{2L} \right] \sin \left[\pi n \frac{A-M}{2L} \right] \exp \left(-\frac{2i\pi n \Delta}{L} \right), \quad (6)$$

where A , L , and M are the sarcomere structural parameters (Fig. 1). Δ is the parameter representing the position of the Gaussian beam on the sample (Fig. 2). The intensity at each position Δ was obtained by integrating the emission profile according to the condenser properties:

$$I(\Delta) = \int_0^{2\pi} \int_0^{\Theta} I(\theta, \phi) \sin \theta d\theta d\phi, \quad (7)$$

where $\Theta = \arcsin(\text{NA}_C)$. Due to the RI mismatch, the emission profile could change in such a way that relevant intensity parts are not collected by the condenser. Moreover, an increased phase-mismatch results in a lower SHG signal, with a less pronounced intensity decrease at the M-band region due to the hemifilament phase reversal, resulting in altered sarcomeric intensity profiles.

3 Results

3.1 Dispersion

To emphasize the effect of the RI mismatch and a free A-band, simulations were performed and compared to a representative experimental profile [Figs. 3(a) and 3(b)]. It is clear that a zero RI mismatch results in simulated profiles that do not agree with the experimental data, neither for $A = 1.6 \mu\text{m}$ and $M = 0.15 \mu\text{m}$ nor for the optimal A and M obtained from a fit. Increasing the RI mismatch to $\Delta n = 0.02$ resulted in theoretical sarcomeric profiles that are closer matching to the experimental data, with the best match obtained for the fitted A- and M-band

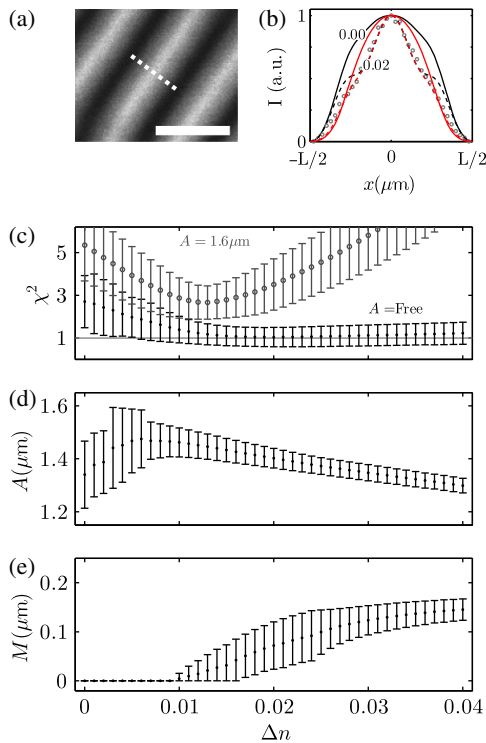


Fig. 3 The effect of dispersion on skeletal sarcomere intensity profiles imaged using NA = 0.8. (a) Typical second harmonic generation (SHG) image of single-band sarcomeric structures. Scale bar 3 μm . The dashed line illustrates a selected profile containing one sarcomere. (b) Typical experimental single-band pattern (circles). The numbers indicate the refractive index mismatch $\Delta n = n_{2\omega} - n_{\omega}$ with n_{ω} fixed at 1.39.²³ Additional simulation parameters: $A = 1.60 \mu\text{m}$ and an $M = 0.15 \mu\text{m}$ for black lines. The red lines show the best fit for each refractive index (RI) mismatch with a free A and M . The profiles are normalized to their maximum value. (c) Effect of preset RI mismatch on the χ^2 of the fit on a set of single-band sarcomere intensity profiles. A freely adjustable A-band (dots) versus an A-band fixed at $1.6 \mu\text{m}$ (circles)⁹ is shown. The error bars represent standard deviation ($N = 16$). (d) and (e) show the resulting A- and M-band lengths, respectively, as functions of the RI mismatch for freely adjustable A and M .

length. Our data indicate that both the RI mismatch and the freely adjustable filament lengths are crucial to obtain simulated profiles properly matching the experimental data.

To gain insight into the effective dispersion properties of striated muscle, a set of single-band sarcomere SHG profiles ($N = 16$) was analyzed using an RI mismatch ranging from 0 to 0.04 with a 0.001 step size [Figs. 3(c)–3(e)]. Assuming that the supramolecular model is an accurate model, the optimal Δn can be determined by means of the resulting χ^2 . In the analysis, the sarcomere length and the M-band size were freely adjustable. Additionally, the effect of taking a freely adjustable A-band parameter was compared to a fixed A-band value. In accordance with Rouède et al.,⁹ this value was chosen as $1.6 \mu\text{m}$. For the freely adjustable A-band length, the minimal $\chi^2 = 1.04 \pm 0.45$ was observed for a $\Delta n = 0.020$. For this optimal RI mismatch, an apparent A-band length of $A = 1.40 \pm 0.04 \mu\text{m}$ was obtained and an apparent M-band length of $M = 0.07 \pm 0.05 \mu\text{m}$ was simultaneously obtained (Table 1). Fixing the A-band length to $1.6 \mu\text{m}$ resulted in a notably higher minimal $\chi^2 = 2.65 \pm 0.78$ at $\Delta n = 0.013$, with an apparent M-band length of $M = 0.04 \pm 0.04 \mu\text{m}$.

Because no significant effects were observed on the recovered parameters for n_{ω} ranging from 1.37 to 1.41, the value of n_{ω} was always fixed at 1.39. This finding indicates that the RI mismatch imposes the major profile alterations, not the effective RI.

3.2 Tight Focusing

The data shown in Fig. 3 were generated using an illumination objective with NA = 0.8. One could argue that a higher NA is beneficial for the resolution, and thus is better to accurately estimate the length parameters. However, tight focusing of the light polarized in the x -direction is known to induce polarization components in both the y and z directions,^{27,28} a feature that is not included in the supramolecular model.⁹ We experimentally tested the effect of increasing the NA to 1.3 by removing the back aperture pinhole and imaging the exact same regions as for the low NA (Fig. 4). Both from the raw image data [Fig. 4(a)] and the profile comparison [Fig. 4(b)], it is clear that tight focusing alters the SHG intensity profile, resulting in pronounced shoulder regions near the sides of the M-band.

The sarcomere dimensions were studied in a similar way as for the moderate NA objective. The PSF was acquired separately and included in the analysis. Compared to the low NA data, a different optimal RI mismatch of $\Delta n = 0.028$ resulted at the minimal $\chi^2 = 2.08 \pm 1.06$. At this RI mismatch, a significantly different apparent $M = 0.03 \pm 0.03 \mu\text{m}$ ($p < 0.005$) and similar apparent $A = 1.38 \pm 0.04 \mu\text{m}$ were observed.

3.3 Myosin Density Distribution

The myosin rod is known to be the basic building block of the myosin thick filament. Using detailed information of these rods, we studied their role in defining the sarcomere SHG intensity profile and the associated lengths estimated by the supramolecular model. The myosin rod can be subdivided into two main regions: the heavy meromyosin (HMM) and the light meromyosin (LMM) region (Fig. 1). The HMM consists of two subfragments: subfragment 1 (S1) containing the two globular heads and the 62 nm long subfragment 2 region (S2), which is part of the α helical coiled-coil of the myosin rod.³⁰ The other part of this α helix is located at the 100.6 nm long LMM region.³⁰ It is known that only the LMMs assemble into the backbone of the thick filament, but how this packing is organized is still under debate.^{19,29,30,33} A general consensus is that the myosin density decreases at the distal parts of the myosin filament.^{19,30} We tested two possible packing schemes, both based on the complete bipolar model suggested by Skubiszak and Kowalczyk³⁰ in which the myosin rod takes a helical form.

For both models, a total of 98 positions with S1 units (crowns) are assumed for the entire thick filament.^{29,30} The step between successive myosin rods is 14.33 nm and the anti-parallel overlap in the central zone is maximal $7 \times 14.33 \text{ nm}$. Due to the helical rod shape, the LMM and S2 have projected axial lengths of 88.44 and 53.17 nm , respectively. In the Skubiszak and Kowalczyk packing model, the three successive proximal and distal crowns of each hemifilament, resulting in a total of 12 out of 98 crowns, contain only one set of globular heads (S1), whereas the remaining crowns contain three of those sets. The thick filament is then composed of a total of 270 myosin rods. The second packing model is based on observations done by Knight et al.²⁹ Each crown has three sets of globular heads and a gap is present before the last two distal crowns.

Table 1 Comparison of apparent A- and M-band lengths between experimentally obtained values in this work, and values obtained by simulations taking the effective myosin density into account. The objective NA = 0.8. All lengths are in μm , and the mean values with standard deviations are given. $N = 250$ for simulations.

Parameter	Experimental	Skubiszak and Kowalczyk ³⁰		Knight ²⁹	
	($N = 16$)	LMM	LMM + S2	LMM	LMM + S2
A	1.40 ± 0.04	$1.31 \pm 0.01^*$	$1.35 \pm 0.01^*$	$1.37 \pm 0.01^*$	1.40 ± 0.01
M	0.07 ± 0.05	$0.03 \pm 0.02^*$	$0.11 \pm 0.01^*$	$0.01 \pm 0.01^*$	0.06 ± 0.02

Note: * denotes $p < 0.001$ compared to experimental value (one-way ANOVA).

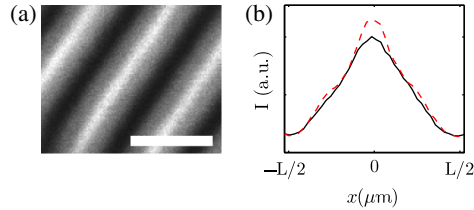


Fig. 4 Effect of tight focussing on the SHG intensity profile. (a) Raw image data obtained using an objective with NA = 1.3 for same region, as shown in Fig. 3(a). (b) Profile comparison of raw data for objective with NA = 0.8 (solid) and NA = 1.3 (dashed). Scalebar $3 \mu\text{m}$.

A total of 294 myosin molecules are then contained in the thick filament.

To calculate the SHG profiles from these packing schemes, the SHG active density $g(x)$ was defined by the sum of polarized rods in the positive and negative x -directions. This means that one side of the filament contains a negative density, the other side is positive, and at the center of the myosin rod, the SHG active density is zero (Fig. 5). This is in agreement with the original supramolecular model.⁹ In Fig. 5, the myosin density $g(x)$ along the thick filament axis is plotted for both models and for the case of LMM or LMM+S2 as the SHG active region. Note that for both packing models, the myosin density turns zero at $\approx 0.8 \mu\text{m}$ (distal) when LMM+S2 is considered, as indicated by the dots in Fig. 5. This explains the $1.6 \mu\text{m}$ observed by EM.

We included the effective myosin rod packing scheme $g(x)$ in the supramolecular model by calculating the Fourier coefficients $a_{\Delta,n}$ through numerical integration of

$$a_{\Delta,n} = \int_{-L/2}^{+L/2} g(x) \exp\left[-\frac{2i\pi n(x + \Delta)}{L}\right] dx. \quad (8)$$

In this adjusted model, the SHG intensity profile is entirely defined by the packing scheme and sarcomere length L , making the A and M parameters of the original model redundant. To be able to compare the simulated profiles based on $g(x)$ to the experimentally obtained profiles, the simulated profiles were analyzed with the original supramolecular model. This yielded A and M values that can be compared to their corresponding experimental values (Table 1).

4 Discussion

The presented work was initiated by the discrepancy between the experimentally obtained apparent A- and M-band lengths,

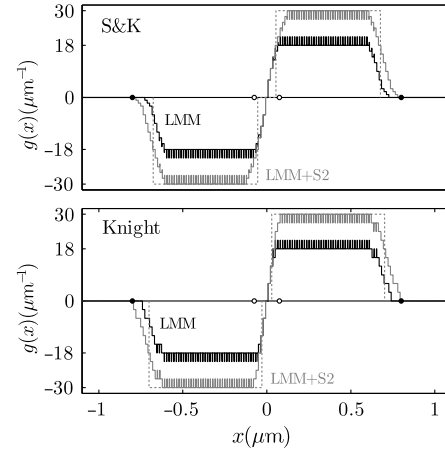


Fig. 5 Plot of SHG active density for each position along the axis of the thick filament $g(x)$, according to the model by Skubiszak and Kowalczyk (S&K) or Knight, either with or without taking the S2 part into account. The polarity inversion at the center of the thick filament is included by the sign of the density. The dashed line represents the best fitting supramolecular model for the case of LMM + S2 as SHG active. The dots and circles indicate the A-band and M-band range, respectively, according to EM observations.¹⁹

and the lengths assumed in the supramolecular model for sarcomere SHG intensity profiles. Both the apparent A- and M-band lengths consistently resulted in values lower than the assumed values. We conclude that when applying the supramolecular model to single-band intensity profiles, the experimentally obtained lengths for the A- and M-bands are $A = 1.40 \pm 0.04 \mu\text{m}$ and $M = 0.07 \pm 0.05 \mu\text{m}$, instead of $A = 1.6 \mu\text{m}$ and $M = 0.15 \mu\text{m}$, respectively. Note that for comparing these values, we assumed no variation of filament lengths across different vertebrate species.³⁴ To explore the observed length differences, the effect of optical parameters of the RI mismatch and objective NA was evaluated. Additionally, the biologically relevant myosin density distribution was explored.

Based on the goodness-of-fit of the supramolecular model to the experimental data [Fig. 3(c)] and visual inspection of the fitted profiles [Fig. 3(b)], our data clearly demonstrate that leaving the A-band freely adjustable resulted in better fits. Although it might be obvious that increasing the degrees of freedom results in better fits, it caused the resulting apparent A-band length to vary around $1.4 \mu\text{m}$, severely deviating from the assumed $1.6 \mu\text{m}$. This indicates that SHG-based data cannot be compared directly to the lengths estimated by other techniques, such as EM.

For the full studied RI mismatch range, and in case of a freely adjustable A , the analysis revealed lower than expected apparent

A- and M-band lengths (Table 1). Regarding the apparent A-band length, the data in Fig. 3(c) show that the expected $1.6 \mu\text{m}$ is never returned by the fit in the studied RI mismatch range. The apparent M-band length for Δn below 0.01 always returned 0, again not agreeing with the initial assumptions of the supramolecular model. The optimal RI mismatch was estimated to be $\Delta n = 0.02$ with $n_o = 1.39$ (Fig. 3). This Δn is lower than previously reported values of ≈ 0.03 , obtained by measurements on fresh tissue.²³ Our sample was fixed with 4% PFA and cryoprotected with 30% sucrose, suggesting that the obtained RI mismatch value is protocol specific and probably limited to the presented experiments. We opted to select the Δn for which the average χ^2 is at its absolute minimal value. Note, however, that for a free A , the χ^2 was acceptably low in a broad range around this minimum. In fact, a t -test with 5% confidence levels revealed that for any RI mismatch < 0.011 , the average χ^2 was not significantly different than 1 in the tested range. This might be related to the low resolution of the used objective (NA = 0.8). For this lower resolution, good fits can be obtained for any higher RI mismatch, but with unexpected values for both A and M . Despite the uncertainty of the method, we chose to continue our work with the RI mismatch for which the average χ^2 is at its absolute minimal value. This choice was further rationalized by the following observation. For increasing Δn , M tends toward a value that agrees with that obtained by EM, indicating that a higher Δn is more suited. However, at a higher Δn , A decreased and deviates even more from the EM value, suggesting a lower Δn is more appropriate. To conclude, we were not able to generally define the effective RI mismatch of fixed muscle tissue with this approach, though we emphasize the importance of taking sample dispersion properties into account when applying the supramolecular model (Fig. 3).

In an attempt to explain the A-band length discrepancy, two previously described models for the myosin rod arrangement within the thick filament were implemented in the supramolecular model. Using this, the influence of the effective myosin density on the parameter recovery by the supramolecular model was tested. For each packing model, both the case of only LMM and LMM + S2 as SHG active regions were considered (Table 1, NA = 0.8). First of all, independent of the used model or of which region should be considered as the SHG active region, the apparent A- and M-band lengths appeared always shorter than their corresponding EM values of 1.6 and $0.15 \mu\text{m}$, respectively. This is in agreement with our experimental results, indicating that the density distribution of the myosin rods is crucial in defining the SHG intensity profile. Regarding both the apparent A- and M-band lengths, only the simulated profiles based on the packing model by Knight et al.,²⁹ with LMM + S2 as SHG active regions resulted in similar lengths as found in the experimental data. This suggests that the S2 region should be taken into account as a significant contributor, a fact that is currently still under debate. Plotnikov et al.¹¹ suggests that only the LMM inside the thick filament backbone is the major contributor. Based on polarization SHG (P-SHG), Psilodimitrakopoulos et al.³⁵ show that the helical pitch angle of the SHG source resembles that of the myosin α -helix of which both the LMM and the S2 region are composed of. Almost simultaneously, but also independent from each other, Nucciotti et al.⁸ and Schürmann et al.³¹ show that the P-SHG profile depends on the contraction state of the sarcomeres. They suggest and simulate that the reorientation of the S2, in part due to binding

of the myosin heads (S1) to actin, is causing a change in P-SHG response, thereby proving that S2 significantly contributes to the SHG signal. To test the effect of the S2 presence on the apparent A-band and M-band lengths, it would be better to effectively remove this region by long-term trypsinization or specific cleaving.³⁶ Alternatively, experiments based on the rigor state of muscle tissue, similar to those by Nucciotti et al.⁸ and Schürmann et al.,³¹ can be performed to study the effect of S2 reorientation on the retrieved lengths.

The effect of the objective NA on the profiles was experimentally tested by imaging regions with both NA = 0.8 and NA = 1.3 (Sec. 3.2). For both NAs, a different optimal RI mismatch and M-band size were observed, while a similar A-band length was returned. The observed differences are possibly due to additional polarization fields caused by the high NA.^{27,28} These fields are not taken into account by the supramolecular model,⁹ yielding different results for the same sarcomeres. Since the high NA describes the experimental data less accurately, as indicated by the higher χ^2 , and because tight focusing is known to alter polarization states, we suggest that a moderate NA is beneficial when using the supramolecular model. However, using this moderate NA comes at the cost of a lower resolution, making accurate estimates of the filament lengths prone to errors. Alternatively, if one desires to use a higher NA, the supramolecular model should be adjusted to include the different field components introduced by the tight focusing. This requires redefining the implementation of the second order susceptibility and Gaussian illumination beam, similar to what Schürmann et al.³¹ did. This would make the model complicated and requires finite-element methods to calculate the intensity profiles. These methods additionally allow to include other optical artifacts, such as the ellipticity of the illumination beam or local changes in the RI,²⁶ probably resulting in more accurate models. Conversely, finite-element methods are based on heavier calculations making high-throughput analyses extremely slow.

By an apparent increase in the apparent M-band size, the supramolecular model is able to distinguish regular sarcomeres from proteolytic ones.⁹ This means that the M-band length is more important than the A-band length as a marker for decreased muscle quality. To overcome possible covariance between M and A as a fit parameter, it is advisable to fix the A-band length to the previously obtained value of $\approx 1.4 \mu\text{m}$ (Table 1). Additionally, due to the lower resolution caused by a moderate NA, the apparent M-band length often reduces to a meaningless value of $0 \mu\text{m}$. A lower limit for the apparent M-band size should then be set to the observed $\approx 0.07 \mu\text{m}$ (Table 1).

Alternative to the apparent increase of the M-band length, a thick filament disorder, which is suggested by Rouède et al.⁹ to be the source of the increasing M-band size, can be directly included into the supramolecular model. This would be more in line with the observations of Gotthardt et al.³⁷ They show data of skeletal muscle fibers with sarcomere disarray due to titin kinase domain absence, which is indicative for muscle degeneration. The disarray is evidenced by a dimmed M-line in electron micrographs, while the data simultaneously show a random shifting of the individual thick filaments. By directly implementing the thick filament disorder, simultaneously occurring effects on the A- and M-band lengths are taken into account (Fig. 6). The disorder can be implemented by replacing Δ in Eq. (6) by $\Delta + \delta$, where δ represents the filament shift with respect to the central position (Fig. 6). The number of myosin

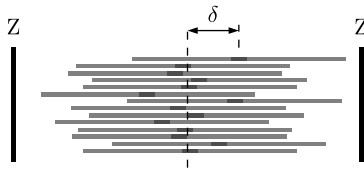


Fig. 6 Depiction of the myosin disorder model with a Gaussian distribution. Each horizontal line represents a thick filament containing the centrosymmetric M-band, indicated by the dark region. The thick filaments are shifted with respect to the sarcomere center (dashed line) by a distance δ , which is assumed to be Gaussian distributed.

thick filaments within the focal volume, thus contributing to the total SHG signal, is sufficiently large (10^3 – 10^4) to represent the filament shifts as a continuous density distribution function $\Phi(\delta)$. The Fourier coefficients [Eq. (6)] are then to be replaced by

$$a'_{\Delta,n} = a_{\Delta,n} \int \exp\left(-\frac{2i\pi n\delta}{L}\right) \Phi(\delta) d\delta. \quad (9)$$

For a set of thick filaments shifted according to a Gaussian distribution with standard deviation σ , the Fourier coefficients $a_{\Delta,n}$ are modulated by $\exp(-2\sigma^2\pi^2n^2/L^2)$. Using this model, the apparent effect of thick filament disorder on the A- and M-band sizes is quantified by only one parameter σ . However, it relies on using correct values for A and M , which can be obtained by the initial supramolecular model using a set of single-band SHG intensity profiles for which $\sigma = 0$. To conclude, the disorder method does not reject the assumption of a fixed thick filament length³⁸ and omits the need of considering apparent changes in the filament lengths.

5 Conclusions

We showed that the dispersion properties of muscle tissue are crucial for the SHG intensity profiles of sarcomeres. Also, when applying the supramolecular model as developed by Rouède et al.,⁹ it is advisable to use moderate NA objectives for which no significant additional polarization states arise. Under these conditions, the apparent A-band length of $1.40 \pm 0.04 \mu\text{m}$ and apparent M-band length of $0.07 \pm 0.05 \mu\text{m}$ proved to be most appropriate to model single-band intensity profiles. As these lengths differ from those observed by EM, the values for both the A- and M-bands determined by EM and SHG microscopy cannot directly be compared to each other. We believe that the results obtained in this work provide insights that are crucial for the application of the supramolecular model to study SHG intensity profiles in striated muscle and eventually to study pathology-induced sarcomere alterations.

Acknowledgments

This research is part of the Interreg EMR IV-A project BioMiMedics (www.biomimedics.org) and is cofinanced by the European Union, local governments, research institutes and SMEs. Support by the BELSPO funded IAP-PAI network P7/05 on Functional Supramolecular Systems (FS2) is acknowledged. The Province of Limburg (Belgium) is acknowledged for financial support within the tUL IMPULS FASE II program, allowing for the upgrading of the laser source used in this work.

References

1. P.-J. Su et al., "The discrimination of type I and type II collagen and the label-free imaging of engineered cartilage tissue," *Biomaterials* **31**(36), 9415–9421 (2010).
2. P. Stoller et al., "Quantitative second-harmonic generation microscopy in collagen," *Appl. Opt.* **42**, 5209–5219 (2003).
3. R. Paesen et al., "Polarization second harmonic generation by image correlation spectroscopy on collagen type I hydrogels," *Acta Biomater.* **10**(5), 2036–2042 (2014).
4. O. Nadiarnykh and P. J. Campagnola, "Retention of polarization signatures in SHG microscopy of scattering tissues through optical clearing," *Opt. Express* **17**, 5794–5806 (2009).
5. P. J. Campagnola and L. M. Loew, "Second-harmonic imaging microscopy for visualizing biomolecular arrays in cells, tissues and organisms," *Nat. Biotechnol.* **21**, 1356–1360 (2003).
6. S. Psilodimitrakopoulos et al., "Estimation of the effective orientation of the SHG source in primary cortical neurons," *Opt. Express* **17**, 14418–14425 (2009).
7. A. C. Kwan, D. A. Dombeck, and W. W. Webb, "Polarized microtubule arrays in apical dendrites and axons," *Proc. Natl. Acad. Sci. U. S. A.* **105**(32), 11370–11375 (2008).
8. V. Nucciotti et al., "Probing myosin structural conformation in vivo by second-harmonic generation microscopy," *Proc. Natl. Acad. Sci.* **107**, 7763–7768 (2010).
9. D. Rouède et al., "Modeling of supramolecular centrosymmetry effect on sarcomeric SHG intensity pattern of skeletal muscles," *Biophys. J.* **101**, 494–503 (2011).
10. G. Recher et al., "Three distinct sarcomeric patterns of skeletal muscle revealed by SHG and TPEF microscopy," *Opt. Express* **17**, 19763–19777 (2009).
11. S. V. Plotnikov et al., "Characterization of the myosin-based source for second-harmonic generation from muscle sarcomeres," *Biophys. J.* **90**, 693–703 (2006).
12. N. G. Laing, Ed., *The Sarcomere and Skeletal Muscle Disease*, Springer, New York (2008).
13. W. Liu, N. Raben, and E. Ralston, "Quantitative evaluation of skeletal muscle defects in second harmonic generation images," *J. Biomed. Opt.* **18**(2), 026005 (2013).
14. P. R. Taub et al., "Perturbations in skeletal muscle sarcomere structure in patients with heart failure and type 2 diabetes: restorative effects of (-)-epicatechinrich cocoa," *Clin. Sci.* **125**(8), 383–389 (2013).
15. C. S. Garbe et al., "Automated multiscale morphometry of muscle disease from second harmonic generation microscopy using tensor-based image processing," *IEEE Trans. Biomed. Eng.* **59**(1), 39–44 (2012).
16. P. Garcia-Canadilla et al., "Automated cardiac sarcomere analysis from second harmonic generation images," *J. Biomed. Opt.* **19**(5), 056010 (2014).
17. C. Odin et al., "Collagen and myosin characterization by orientation field second harmonic microscopy," *Opt. Express* **16**, 16151–16165 (2008).
18. T. Boulesteix et al., "Second-harmonic microscopy of unstained living cardiomyocytes: measurements of sarcomere length with 20-nm accuracy," *Opt. Lett.* **29**, 2031–2033 (2004).
19. J. Squire, "General model of myosin filament structure: III. molecular packing arrangements in myosin filaments," *J. Mol. Biol.* **77**(2), 291–323 (1973).
20. M. Sjöström and J. M. Squire, "Fine structure of the A-band in cryo-sections: The structure of the A-band of human skeletal muscle fibres from ultra-thin cryo-sections negatively stained," *J. Mol. Biol.* **109**(1), 49–68 (1977).
21. R. LaComb et al., "Phase matching considerations in second harmonic generation from tissues: Effects on emission directionality, conversion efficiency and observed morphology," *Opt. Commun.* **281**(7), 1823–1832 (2008).
22. J. J. J. Dirckx, L. C. Kuypers, and W. F. Decraemer, "Refractive index of tissue measured with confocal microscopy," *J. Biomed. Opt.* **10**(4), 044014 (2005).
23. T. Vo-Dinh, *Biomedical Photonics Handbook*, CRC Press, Boca Raton, Florida (2003).
24. A. N. Bashkatov, E. A. Genina, and V. V. Tuchin, "Optical properties of skin, subcutaneous, and muscle tissues: a review," *J. Innovative Opt. Health Sci.* **04**(01), 9–38 (2011).

25. R. W. Boyd, *Nonlinear Optics*, 3rd ed., Elsevier Inc., London (2008).
26. V. Ratan, *Handbook of Human Physiology*, Jaypee Brothers, Medical Publishers, New Delhi (2004).
27. A. A. Asatryan, C. J. R. Sheppard, and C. M. de Sterke, "Vector treatment of second-harmonic generation produced by tightly focused vignetted gaussian beams," *J. Opt. Soc. Am. B* **21**, 2206–2212 (2004).
28. E. Yew and C. Sheppard, "Effects of axial field components on second harmonic generation microscopy," *Opt. Express* **14**, 1167–1174 (2006).
29. P. Knight et al., "Distribution of mass within native thick filaments of vertebrate skeletal muscle," *J. Mol. Biol.* **189**(1), 167–177 (1986).
30. L. Skubiszak and L. Kowalczyk, "Myosin molecule packing within the vertebrate skeletal muscle thick filaments: a complete bipolar model," *Acta Biochim. Pol.* **49**(4), 829–840 (2002).
31. S. Schürmann et al., "Second harmonic generation microscopy probes different states of motor protein interaction in myofibrils," *Biophys. J.* **99**(6), 1842–1851 (2010).
32. D. Rouède et al., "Theoretical and experimental SHG angular intensity patterns from healthy and proteolysed muscles," *Biophys. J.* **104**(9), 1959–1968 (2013).
33. R. Craig and G. Offer, "Axial arrangement of crossbridges in thick filaments of vertebrate skeletal muscle," *J. Mol. Biol.* **102**(2), 325–332 (1976).
34. T. Burkholder and R. Lieber, "Sarcomere length operating range of vertebrate muscles during movement," *J. Exp. Biol.* **204**(9), 1529–1536 (2001).
35. S. Psilodimitrakopoulos et al., "Polarization dependant in vivo second harmonic generation imaging of *Caenorhabditis elegans* vulval, pharynx, and body wall muscles," *Proc. SPIE* **6860**, 686008 (2008).
36. M. S. Miller et al., "Alternative S2 hinge regions of the myosin rod affect myofibrillar structure and myosin kinetics," *Biophys. J.* **96**(10), 4132–4143 (2009).
37. M. Gotthardt et al., "Conditional expression of mutant M-line titins results in cardiomyopathy with altered sarcomere structure," *J. Biol. Chem.* **278**(8), 6059–6065 (2003).
38. H. Sosa et al., "Ultrastructure of skeletal muscle fibers studied by a plunge quick freezing method: myofilament lengths," *Biophys. J.* **67**(1), 283–292 (1994).

Biographies for the authors are not available.